

Atomic Monte-Carlo Simulation for CBRAM with Various Filament Geometries

Y.D. Zhao, P. Huang*, Z.H. Guo, Z.Y. Lun, B. Gao, X.Y. Liu, J.F. Kang[†]

Institute of Microelectronics
 Peking University
 Beijing, China
 *phwang@pku.edu.cn, [†]kangjf@pku.edu.cn

Abstract—An atomic Monte-Carlo simulator of Conductive Bridge Random Access Memory (CBRAM) is developed to investigate the microscopic properties of filament growth and dissolution during Forming/SET and RESET processes. The cluster growth during nucleation correlated with electrochemical reactions and cations transportation are included. The impacts of the critical material parameters on the geometry of conductive filaments (CF) are clarified by the simulator. The conical and dendrite shape CF experimentally observed by different groups are simulated by tuning the critical material parameters. Using the simulator, the microscopic properties of Forming/SET and RESET processes with different CF geometries are investigated and the retention behaviors can be analyzed.

Keywords—RRAM, resistive switching, conductive filament, conductive bridge, Monte-Carlo, simulation.

I. INTRODUCTION

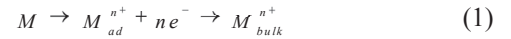
CBRAM is a promising candidate among the emerging non-volatile memory technologies due to its excellent scaling and low power potential [1-8]. By selecting different metal and electrolyte materials, various CF geometries have been visualized by in-situ TEM and AFM observations [1-6]. Nevertheless, the critical issues such as the impacts of materials on CF geometry remain unaddressed. Moreover, the simulation of RESET process is still limited in the literature, bringing difficulty to clarify the underlying physics of CF dissolution.

In this paper, an atomic Monte-Carlo simulator of CBRAM is developed to bridge the microscopic and electrical characteristics during switching processes including the Forming/SET and RESET processes. The experimental observed conical or dendrite CF reported by different groups are simulated and reproduced by the simulator, just by tuning the critical material parameters. The simulation results reveal the CF dissolution region during RESET process of different CF geometries. Using the simulation tool, the retention behaviors of CBRAM are also studied.

II. SIMULATION METHODS

A typical CBRAM device consists of a solid-electrolyte layer sandwiched between an active electrode (Ag or Cu) and an inert electrode. Fig. 1 illustrates the microscopic behaviors and the correlated physical effects during resistive switching,

which include 1) metal atoms oxidation into cations from active electrode or filament



where M represents metal atoms, M_{ad}^{n+} is the adsorbed cations, M_{bulk}^{n+} is the cations in the bulk. The oxidation probability can be described as [9]

$$P_{ox} = f \cdot \exp(-(E_{ox} - \Delta\phi) / k_B T) \quad (2)$$

where f is the vibration frequency, E_{ox} is the activation energy of oxidation, T is the local temperature, and $\Delta\phi$ is the barrier height reduction induced by electric field.

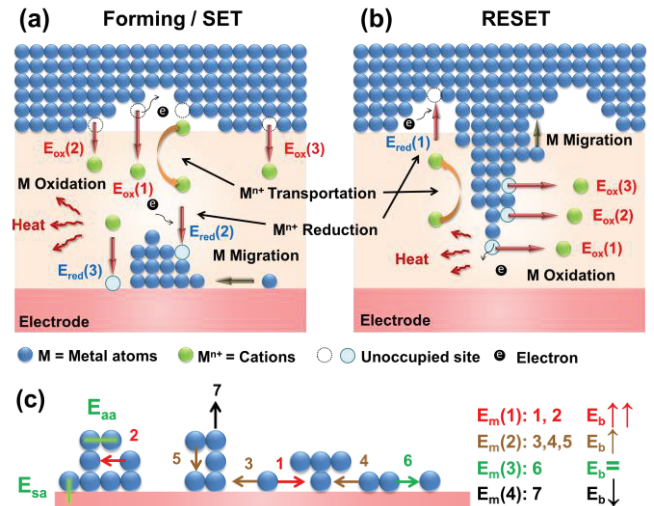


Fig. 1 Microscopic behaviors and correlated physical effects during resistive switching processes (a) for SET or Forming, (b) for RESET (conical shape filament as an example). (c) Metal atoms migration to the minimum energy locations.

2) cations transportation in electrolyte, with probability of [10]

$$P_h = f \cdot \exp(-E_h - \Delta\phi) / k_B T) \quad (3)$$

where E_h is the hopping barrier of cations.

3) cations reduction into metal atoms



whose probability is [9]

$$P_{red} = f \cdot \exp(-(E_{red} - \Delta\phi) / k_B T) \quad (5)$$

where E_{red} is activation barrier of reduction.

4) metal atoms migration to the minimum energy locations. In Fig. 1(c), E_{sa} and E_{aa} represent the bond energy within substrate/atom and atom/atom respectively. The migration rate of metal atoms $E_m(1-4)$ depends on the increase of the filament bond energy (E_b), where $E_m(1-2)$ and $E_m(4)$ represent the atom aggregation and detachment, respectively. The migration probability can be described as [9]

$$P_m = f \cdot \exp(-E_m / k_B T) \quad (6)$$

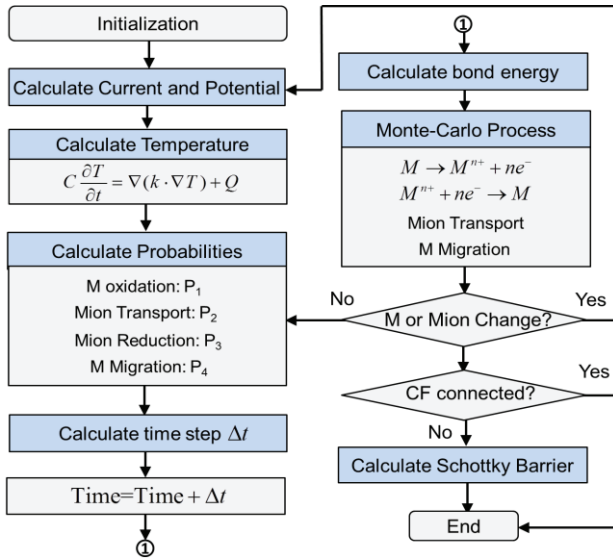


Fig. 2 Simulation flowchart of the developed Monte-Carlo simulator.

Based on the physical effects, an atomic Monte-Carlo simulator is developed to feature the RS processes and the correlated microscopic properties of CBRAM. Fig. 2 shows the simulation flow chart. In the beginning of the simulation, the device thickness and the initial distributions of metal atoms and cations are extracted as inputs. Then the potential and current distributions in metal and electrolyte layers are calculated. Based on the current and potential, the local temperature distribution of the device is calculated by the Fourier heat-flow equation [10]

$$C \frac{\partial T}{\partial t} = \nabla \cdot (k \cdot \nabla T) + Q \quad (7)$$

where C represents the specific heat per unit volume, k is the thermal conductivity of metal or electrolyte layer, and Q is the Joule heat power density.

After that, the probabilities of atoms oxidation, cations transportation, cations reduction and atoms migration are calculated based on equations (2), (3), (5) and (6). Then the time is updated. By using Monte-Carlo methods, the next physical process can be decided based on the probabilities. The Schottky barrier in the device is considered by serially connecting a diode, which is decided by the contact of electrodes and electrolyte [11].

The above calculations will be repeated as the sweeping voltage changes. The critical simulation parameters used in the simulator are listed in Table I, which are calibrated by the experiment in Ref.[1].

Table I Parameters used in the simulator

parameter	value	parameter	value
vibration frequency: f	10^{13} Hz	R_2 (electrolyte)	$5 \times 10^{12} \Omega$
oxidation barrier: E_{ox} (1)a, (2)s, (3)v	0.9, 1.0, 1.2 eV	R_3 (cation)	$5 \times 10^6 \Omega$
reduction barrier: E_{red} (1)v, (2)s, (3)a	0.5, 0.7, 1.3 eV	R_4 (vacancy)	$5 \times 10^{12} \Omega$
migration barrier: E_m (1), (2), (3), (4)	0.6, 0.8, 1.2, 2 eV	thermal conductivity: $k1^*$, $k2^{\#}$	20, $2 W/K \cdot m$
bulk hopping barrier: $E_R(1)^*$, (2)#	1.3, 1.3 eV	specific heat per unit volume: C	$2.4 \times 10^6 J/K \cdot m^3$
interface hopping barrier: $E_I(1)^*$, (2)#	1.3, 1.3 eV	device length: l	60nm
R_1 (metal)	$5 \times 10^6 \Omega$	device thickness: $d1^*$, $d2^{\#}$	20nm, 10nm

Note: *:metal layer, #: electrolyte layer, a: adatom, s: step, v: vacancy

III. RESULTS AND DISCUSSIONS

The conical and dendrite CF geometries observed by experiments [1-3] are reproduced by adopting different material parameters in the simulator. Fig. 3, 5, 6 demonstrate CF evolution and dissolution of three typical CF geometries. As shown in Fig. 3(a), a conical CF with top wide is simulated with the parameters listed in Table I, which is consistent with experimental AFM tomography after SET process [1]. The simulated CF configuration after RESET is shown in Fig. 3(b), which indicates the dissolution region of CF locating at the thinnest part due to thermal-electric effect, and the corresponding potential and temperature distributions during RESET are shown in Fig. 3(c). The good agreement of the simulated and measured I-V curves of the device is achieved as shown in Fig. 4.

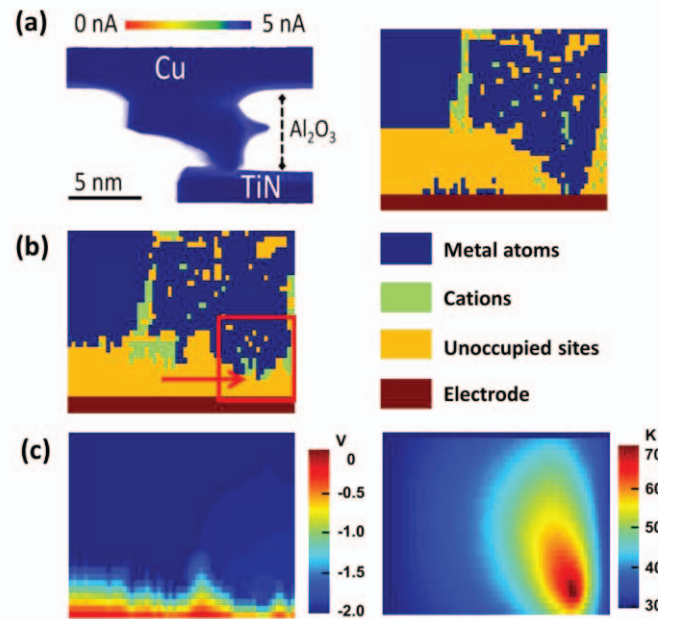


Fig. 3 (a) Comparison of simulated CF with experimental observation by AFM of Cu/Al₂O₃/TiN after SET. (b) Simulated CF configuration after RESET. (c) Potential (under 2V) and temperature distributions during RESET.

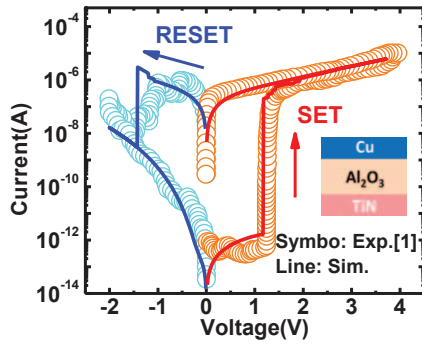


Fig. 4 Measured and simulated I-V curves during SET and RESET in Cu/Al₂O₃/TiN device.

Conical CF with bottom wide is simulated as shown in Fig. 5, where the material parameters are listed in Fig. 5(d). The evolution and dissolution of CF are shown in Fig. 5(a) and (b), which are in accordance with the observed TEM images in Ref.[2]. In this case, the dissolution region during RESET locates near the active electrode, which is the thinnest part of CF. The potential and temperature distributions during RESET are shown in Fig. 5(c). Based on the simulations, the critical parameters E_{ox} , E_h and E_{red} are identified to influence CF geometry and the proper parameters are selected to reproduce the targeted CF geometry. When E_{ox} is small compared to E_h , conical CF with top wide is reproduced. When E_h is small compared to E_{ox} and E_{red} , conical CF with bottom wide is developed. As shown in Fig. 5, the high cation mobility in Cu-doping electrolyte (low E_h) leads to CF geometry with bottom wide.

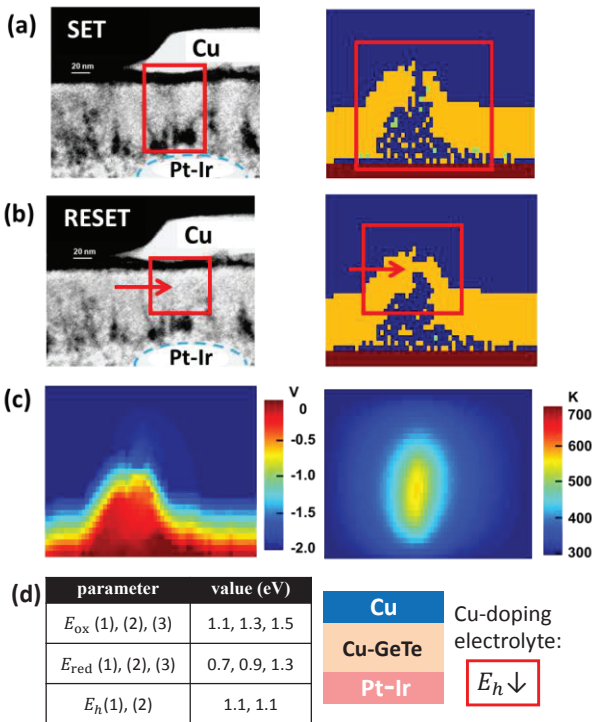


Fig. 5 Comparison of simulated CF with TEM images of Cu/Cu-GeTe/Pt-Ir [2] after SET (a) and RESET (b). (c) The simulated potential (under 2V) and temperature distributions during RESET. (d) The parameters used in this simulation.

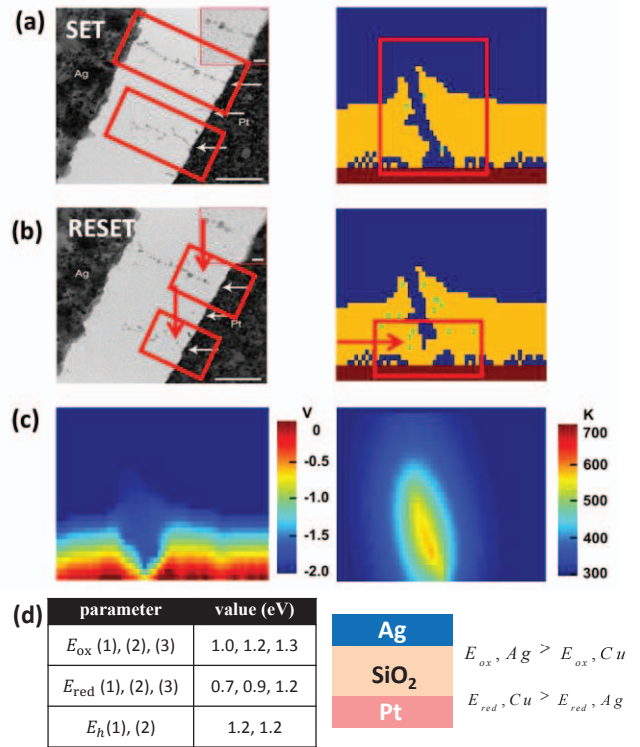


Fig. 6 Comparison of simulated CF with TEM images of Ag-SiO₂-Pt [3] after SET (a) and RESET (b). (c) The simulated potential (under 2V) and temperature distributions during RESET. (d) The parameters used in this simulation.

The balance of E_{ox} , E_h and E_{red} bring in a uniform CF as shown in Fig. 6, which corresponds to dendrite CF observed in TEM images from Ref.[3]. The evolution and dissolution of the uniform CF are shown in Fig. 6(a) and (b), and the potential and temperature distributions during RESET are shown in Fig. 6(c). As shown in Fig. 6(d), devices composed of Ag electrode and electrolyte with low cation mobility tend to generate uniform CFs. Likewise, devices composed of Cu electrode and electrolyte with high cation mobility are likely to generate uniform CFs.

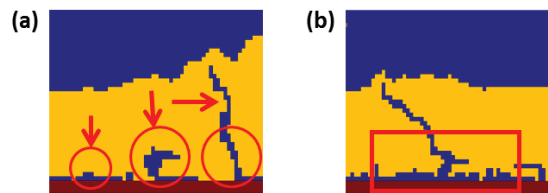


Fig. 7 Simulated CF geometry correlated with material parameters (a) for $E_{aa} > E_{sa}$, isolated island growth. (b) for $E_{aa} < E_{sa}$, nucleation by coalescence of islands.

As has been demonstrated in part II, the bond energy can influence the migration of metal atoms. During Forming process, the growth of atom clusters depends on the bond energy between substrate and atom as shown in Fig. 7. When $E_{aa} > E_{sa}$, the CFs grow in isolated islands. When $E_{aa} < E_{sa}$, the CFs grow by coalescence of islands. The Forming voltage is related with the thickness and thermal conductivity of electrolyte material as shown in Fig. 8. Fig. 9 shows the impacts of E_{ox} , E_h and E_{red} on the Forming voltage.

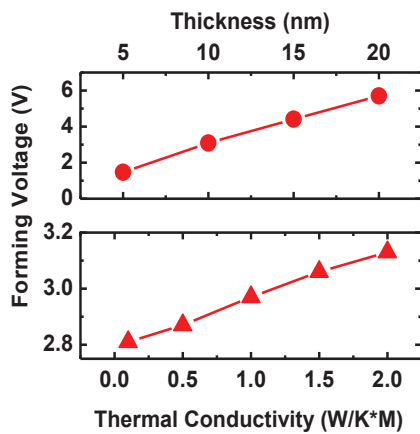


Fig. 8 Forming voltage increases with thickness and thermal conductivity of electrolyte.

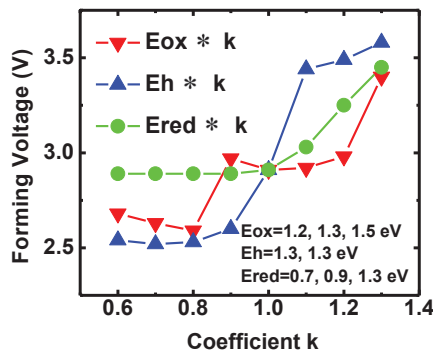


Fig. 9 The relation between forming voltage and the parameters related with CF geometry.

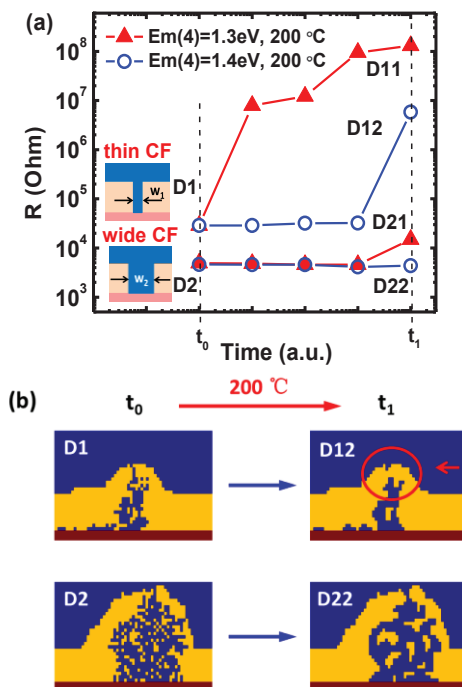


Fig. 10 (a) 200°C LRS retention for different CF widths. (b) Microscopic evolutions of CF configurations in t_0 - t_1 .

The reliability issues can be discussed with the developed simulation tool. The high temperature retention behaviors of CBRAM with different CF widths are simulated as shown in Fig. 10. CF widths are controlled by compliance current during SET. Wide CF controlled by large SET current demonstrates better low resistance state (LRS) retention than thin CF, where structure relaxation results in the rupture of CF. The structure relaxation is controlled by parameters E_m , and dendritic CFs become smooth through edge relaxation.

IV. CONCLUSION

An atomic simulation method is developed to simulate the RS behaviors and microscopic processes of CBRAM. Critical material parameters related with CF geometry are identified by the simulator. Various CF geometries observed in experiments are reproduced by selecting proper simulation parameters. The RESET behaviors of CBRAM with different CF geometries are investigated. Moreover, the simulator can be used to predict the retention behaviors for future device optimization.

ACKNOWLEDGMENT

This work is partly supported by NSFC Program (61421005/61334007) and Beijing Municipal Science and Technology Plan Projects.

REFERENCES

- [1] U. Celano, L. Goux, A. Belmonte, *et al.*, "Conductive-AFM tomography for 3D filament observation in resistive switching devices," in *Proc. IEEE IEDM*, Dec. 2013, pp. 574-577.
- [2] S.-J. Choi, G.-S. Park, K.-H. Kim, *et al.*, "In Situ Observation of Voltage-Induced Multilevel Resistive Switching in Solid Electrolyte Memory," *Adv. Mater.*, vol. 23, pp. 3272-3277, Nov. 2011.
- [3] Y. Yang, P. Gao, S. Gaba, *et al.*, "Observation of conducting filament growth in nanoscale resistive memories," *Nat. Commun.*, vol. 3, pp. 732, Mar. 2012.
- [4] X. Guo, C. Schindler, S. Menzel, *et al.*, "Understanding the switching-off mechanism in Ag^+ migration based resistively switching model systems," *Appl. Phys. Lett.*, vol. 91, pp. 133513, Sep. 2007.
- [5] M. Arita, A. Takahashi, Y. Ohno, *et al.*, "Switching operation and degradation of resistive random access memory composed of tungsten oxide and copper investigated using in-situ TEM," *Sci. Rep.*, vol. 5, pp. 17103, Nov. 2015.
- [6] Q. Liu, J. Sun, H. Lv, *et al.*, "Real-Time Observation on Dynamic Growth/Dissolution of Conductive Filaments in Oxide-Electrolyte-Based ReRAM," *Adv. Mater.*, vol. 24, pp. 1844-1849, Apr. 2012.
- [7] J. Guy, G. Molas, E. Vianello, *et al.*, "Investigation of the physical mechanisms governing data-retention in down to 10nm Nano-trench $Al_2O_3/CuTeGe$ Conductive Bridge RAM (CBRAM)," in *Proc. IEEE IEDM*, Dec. 2013, pp. 742-745.
- [8] A. Redolff, L. Goux, N. Jossart, *et al.*, "A novel CBRAM integration using subtractive dry-etching process of Cu enabling high-performance memory scaling down to 10nm node," in *Proc. IEEE Symp. VLSI Technol.*, Jun. 2015, pp. 134-135.
- [9] X. Guan, S. Yu, H.-S. P. Wong, *et al.*, "On the switching parameter variation of metal-oxide RRAM—Part I: Physical modeling and simulation methodology," *IEEE Tran. Electron Devices*, vol. 59, no. 4, pp. 1172-1182, Apr. 2012.
- [10] P. Huang, B. Gao, B. Chen, *et al.*, "Stochastic Simulation of Forming, SET and RESET Process for Transition Metal Oxide-based Resistive Switching Memory," in *Proc. IEEE SISPAD*, Sep. 2012, pp. 312-315.
- [11] Y. D. Zhao, P. Huang, Z. Chen, *et al.*, "Simulation of TaO_x -RRAM with Ta_2O_{5-x}/TaO_{2-x} Stack Engineering," in *Proc. IEEE SISPAD*, Sep. 2015, pp. 285-288.